

Non-equilibrium quantum dynamics after local quenches

Uma Divakaran ¹, Ferenc Iglói ^{2,3}, Heiko Rieger ¹

¹ Theoretische Physik, Universität des Saarlandes, 66041 Saarbrücken, Germany

² Research Institute for Solid State Physics and Optics, H-1525 Budapest, P.O.Box 49, Hungary

³ Institute of Theoretical Physics, Szeged University, H-6720 Szeged, Hungary

Abstract. We study the quantum dynamics resulting from preparing a one-dimensional quantum system in the ground state of initially two decoupled parts which are then joined together (local quench). Specifically we focus on the transverse Ising chain and compute the time-dependence of the magnetization profile, $m_l(t)$, and correlation functions at the critical point, in the ferromagnetically ordered phase and in the paramagnetic phase. At the critical point we find finite size scaling forms for the nonequilibrium magnetization and compare predictions of conformal field theory with our numerical results. In the ferromagnetic phase the magnetization profiles are well matched by our predictions from a quasi-classical calculation.

PACS numbers: 64.70.Tg, 05.70.Ln, 75.10.Pq, 75.40.Gb

1. Introduction

Recently there has been an increased interest in nonequilibrium relaxation processes in closed quantum systems following a sudden change of the parameters of the Hamiltonian (quantum quench) [1, 2, 3, 4, 5, 6, 7, 17, 8, 9, 10, 11, 12, 13, 14, 15, 16, 18, 19, 20]. Theoretically during the initial period ($t < 0$) the system is described by a Hamiltonian \mathcal{H}_0 with ground state $|\Psi_0\rangle$, which is suddenly changed to a new Hamiltonian, \mathcal{H} , for time $t \geq 0$. The new state of the system - in the Schrödinger picture - is time-dependent:

$$|\Psi(t)\rangle = \exp(-it\mathcal{H})|\Psi_0\rangle, \quad (1)$$

and so is with an operator, say \mathcal{O} , which is expressed at time $t > 0$ in the Heisenberg picture as:

$$\mathcal{O}(t) = \exp(-it\mathcal{H})\mathcal{O}\exp(it\mathcal{H}). \quad (2)$$

Generally one is interested in the relaxation of the local order-parameter,

$$m_r(t) = \langle \Psi_0 | \mathcal{O}_r(t) | \Psi_0 \rangle, \quad (3)$$

at site, r or the time-dependence of the autocorrelation function:

$$G_r(t, t') = \langle \Psi_0 | \mathcal{O}_r(t) \mathcal{O}_r(t') | \Psi_0 \rangle. \quad (4)$$

After long times, $t \gg 1$, the system is expected to relax to a stationary state, in which one measures the correlation function:

$$C_t(r_1, r_2) = \langle \Psi_0 | \mathcal{O}_{r_1}(t) \mathcal{O}_{r_2}(t) | \Psi_0 \rangle. \quad (5)$$

Most often one considers global quenches, when the parameters are modified uniformly at all points of the sample. Experimentally this process can be realized with ultracold atomic gases in optical lattices [21, 22, 23, 24]. After a global quench a quantum system is expected to relax to a thermal (or thermal-like) state, such that the local magnetization (as well as the autocorrelation function) vanishes exponentially, $m_r(t) \sim \exp(-t/\tau)$, with a relaxation (or phase coherence) time τ . Similarly, the correlation function in the stationary state behaves as:

$$C_t(r_1, r_2) \sim \exp(-|r_1 - r_2|/\xi), \quad (6)$$

with a finite non-equilibrium correlation length, ξ . This thermalization of the system is generally explained in terms of quasi-particles [5, 25], which are emitted during the quench at each point of the sample and which travel with a constant velocity, v . Quasi-particles which are originated at nearby sites (which are within the correlation length) are quantum entangled, but other quasi-particles are incoherent. Incoherent particles reaching a reference point, r , will result in the reduction of the value of a local observable and this process is responsible for the exponential decay of the (auto)correlation function. In a system with boundaries these quasi-particles are reflected at the boundaries, which results in more complicated time-dependence, among others reconstruction of the local magnetization [19].

Besides global quenches one also considers local quenches, when the parameters are modified only at a restricted region of the system [26, 27]. Experimentally this type of problem can be realized in the x-ray absorption problem in metals [29], where the creation of a hole plays the role of a local defect and when a conduction electron fills the hole this potential is suddenly switched off. Nonequilibrium dynamics following a local quench has been first studied in the context of the entanglement entropy, \mathcal{S} , in critical quantum spin chains [26, 27, 28]. If we consider two disconnected half chains for time $t < 0$, which are suddenly joint together for $t \geq 0$, then the time-evolution of the entanglement entropy of the two half chains is found to evolve in time asymptotically as:

$$\mathcal{S}(t) = \frac{c}{3} \log t + c_1 , \quad (7)$$

where c is the central charge of the Virasoro algebra and c_1 is a non-universal constant. In view of Eq.(7) basic informations about the critical properties of quantum spin chains, such as the value of the central charge, can be obtained through nonequilibrium local quench dynamics. The result in Eq.(7), which has been first obtained numerically for a free-fermion model [26], has been derived through conformal invariance [27]. It has also been generalized for different positions of the defect [26, 27], as well as for varying strength of the defect in quantum Ising and XX-chains [30]. For a large finite chain of total length, L , the appropriate expression is conjectured to be [30]:

$$\mathcal{S}_L(t) = \frac{c}{3} \log \left| \frac{L}{\pi} \sin \frac{\pi t}{L} \right| + c_1 . \quad (8)$$

The conformal mapping, which has been used for the calculation of the entanglement entropy can be applied [27] to study the time-dependence of one-point functions (such as the local magnetization in Eq.(3)), as well as two-point functions (such as the correlation function in Eq.(5)) in a critical quantum spin chain. In contrary to global quenches these results indicate a power-low relaxation as well as power-low type correlations in the stationary state. This is understandable within the quasi-particle picture, since at a local quench the quasi-particles are expected to be emitted only at a restricted region of the sample and therefore these are quantum entangled. If these quasi-particles arrive after time t to different positions of the chain, say r_1 and r_2 , will result in correlations.

Besides the conformal results which are mentioned above several problems connected with local quench dynamics are still unexplored. To our knowledge there are no numerical investigations, which could be used to check the validity of the conformal conjectures. There are no results about the autocorrelation function and no information is known about nonequilibrium relaxation following a local quench to the ordered or to the disordered phase of a quantum spin chain. In this paper we aim to fill this gap and perform detailed numerical investigations about these open questions. As a model we use the transverse Ising spin chain, which is a prototypical quantum system having ordered and disordered phases as well as a quantum critical point [31]. Using free-fermionic techniques [32, 33, 31] we have studied numerically the nonequilibrium relaxation processes for the magnetization, the autocorrelation and the

equal-time correlation function in large finite systems. Most of our investigations are performed at the quantum critical point, so that we could compare our results with the conformal predictions. However, we also studied quenches to the ordered and to the disordered phases and these results are then compared with semi-classical calculations..

The structure of the paper is the following. The model and the numerical method of the calculation is introduced in Sec.2. Results of the calculations at the critical point, in the ferromagnetic and in the paramagnetic phases are presented in Sections 3, 4 and 5, respectively. Our conclusions are summarized in Sec.6.

2. Model

The system we consider in this paper is the transverse Ising chain of finite length L with open boundaries defined by the Hamiltonian:

$$\mathcal{H} = -\frac{1}{2} \left[\sum_{l=1}^{L-1} J_l \sigma_l^x \sigma_{l+1}^x + \sum_{l=1}^L h_l \sigma_l^z \right], \quad (9)$$

in terms of the Pauli-matrices $\sigma_l^{x,z}$ at site l and bond strengths J_l , which are all equal $J_l = 1$ except the central bond $J_{L/2}$, which is $J_{L/2} = 0$ for time $t \leq 0$. Similarly, the transverse fields are homogeneous, $h_l = h$, except at the central sites, which are $h_{L/2} = h_{L/2+1} = 0$ for time $t \leq 0$ for fixed-spin boundary conditions. (For free-spin boundary conditions these are $h_{L/2} = h_{L/2+1} = h$ for time $t \leq 0$, too.) Generally we measure distances from the defect and use the variable:

$$r = l - \frac{L}{2}. \quad (10)$$

The order-parameter operator of the system is, σ_l^x , what should be inserted in the formulae of the autocorrelation and the correlation functions, see in Eqs.(4) and (5), respectively. For the local magnetization in Eq.(3) one should have: $m_r(t) = \lim_{b \rightarrow 0^+} {}_b \langle \Psi_0 | \sigma_r^x(t) | \Psi_0 \rangle_b$, where $|\Psi_0\rangle_b$ is the ground state of the initial Hamiltonian (9) in the presence of an external longitudinal field b . According to [34] this can be written as the off-diagonal matrix-element of the Hamiltonian (9):

$$m_r(t) = \langle \Psi_0 | \sigma_r^x(t) | \Psi_1 \rangle, \quad (11)$$

where $|\Psi_1\rangle$ is the first excited state of the initial Hamiltonian ($t < 0$). For fixed-spin boundary condition the ground-state is exactly degenerate with $|\Psi_1\rangle$. In the initial state and in the thermodynamic limit, $L \rightarrow \infty$, there is spontaneous ferromagnetic order in the system, $m_r(0) > 0$, for $h < h_c = 1$. On the contrary, for stronger transverse fields, $h > h_c$, the magnetization is vanishing. At the quantum critical point the magnetization vanishes as a power-law: $m_r(0) \sim L^{-x}$, for bulk spins: $r = O(1)$, and $m_{\pm L/2}(0) \sim L^{-x_s}$, for surface spins. Here the magnetization exponent x and the surface magnetization exponent x_s is known exactly: $x = 1/8$ and $x_s = 1/2$.

The Hamiltonian in Eq.(9) can be expressed in terms of free fermions [32, 33, 31], which has been used in previous studies of its non-equilibrium properties [35, 18, 19]. The magnetization profile, as well as the (auto)correlation functions can be expressed

in terms of Pfaffians, which are then evaluated as the square-root of an antisymmetric matrix, which has a rank $O(L)$. In the following Sections we use these techniques to calculate different nonequilibrium quantities.

3. Local quenches at the critical point

3.1. Conformal field theory - a reminder

Here we recapitulate the basic results by Calabrese and Cardy [27] about the use of conformal field theory for local quenches at the critical point. The system is represented in a space-time region with coordinates: (r, t) and the two parts of the chain are decoupled for $t < 0$ and these are joined at $t = 0$ and we measure the properties of the system at $t > 0$. In the path integral formalism one introduces damping factors: $\exp(-\epsilon\mathcal{H})$, so that in Eq.(2) we have $\exp(-it\mathcal{H}) \rightarrow \exp(-it\mathcal{H} - \epsilon\mathcal{H})$ and $\exp(it\mathcal{H}) \rightarrow \exp(it\mathcal{H} - \epsilon\mathcal{H})$. For computational simplicity the operators are inserted at imaginary times: $\tau = it$ and one works in the complex plane $z = r + i\tau$. Here, due to the local quench we have two cuts starting at $\pm i\epsilon$ and ending at $\pm i\infty$. This is represented in the left panel of Fig.1.

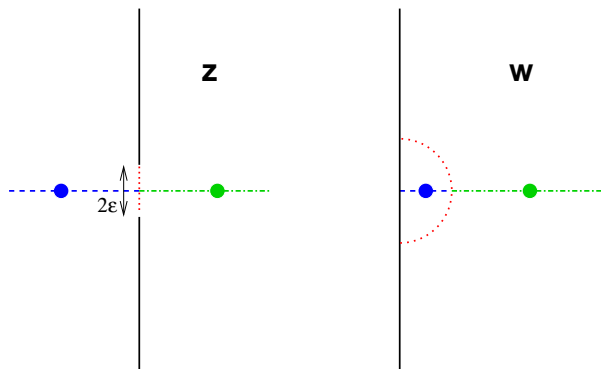


Figure 1. (Color online) Space-time region $z = r + i\tau$ with two cuts starting at $\pm i\epsilon$ (left) which is mapped to the half-plane w through the conformal transformation in Eq.(12). At the end of the calculation one should take $\tau \rightarrow it$.

This geometry is mapped by the Joukowski transformation:

$$w = \frac{z}{\epsilon} + \sqrt{\left(\frac{z}{\epsilon}\right)^2 + 1}, \quad z = \epsilon \frac{w^2 - 1}{2w}, \quad (12)$$

into the half plane, $\text{Re } w > 0$. At the boundaries of the slits in the z -plane as well as at the surface of the w -plane one should impose boundary conditions, which can be either free or fixed spin boundary conditions. In the w -plane the asymptotic form of the one- and two-point functions are generally known due to conformal invariance [36, 37, 38, 40]. These results are then transformed back to the z plane and at the end of the calculation one analytically continues the final result as $\tau \rightarrow it$.

We note that the conformal results obtained in this way are valid for infinitely long chains, i.e. for $L \rightarrow \infty$.

3.2. Magnetization

We have calculated the relaxation of the magnetization in the transverse-field Ising chain following a local quench starting with two different type of initial state. First, we consider an initial state with fixed spins at the defect, in which case the initial defect magnetization stays finite. In this type of setting one can make a direct comparison with the conjectures of conformal invariance. In the second type of calculation in the initial state we use free boundary conditions at the defect. Then we calculate the time-dependence of the off-diagonal order-parameter in Eq.(11), which has a vanishing initial value at the defect in the thermodynamical limit.

3.2.1. Fixed-spin boundary condition In this section in the initial state, $t < 0$, the two half chains are prepared with fixed spins at the boundaries: $\langle \sigma_{L/2}^x \rangle = \langle \sigma_{L/2+1}^x \rangle = 1$, which is obtained by fixing $h_{L/2} = h_{L/2+1} = 0$ in the Hamiltonian in Eq.(9). We use the superscript, $(+)$, to refer for fixed-spin boundary condition. The magnetization profile in the initial state is known from conformal invariance [37, 38]:

$$m_r^{(+)}(t=0, L) \sim \left| \frac{L}{2\pi} \sin \pi \frac{2r}{L} \right|^{-x} \left(\cos \pi \frac{r}{L} \right)^{x_s}, \quad (13)$$

which behaves close to the defect: $m_r^{(+)}(t=0) = A|r|^{-x}$, $|r| \ll L/2$. This is the well-known result by Fisher and de Gennes [39].

After the local quench, for $t > 0$, we take $h_{L/2} = h_{L/2+1} = 1$ (and $J_{L/2} = 1$) and study the evolution of the magnetization. In the limit $|r| \ll L/2$ the conformal mapping in the Sec.3.1 leads to the result [27]:

$$m_r^{(+)}(t) = \begin{cases} A|r|^{-x} & t < r, \\ A \left(\frac{\epsilon}{t^2 - r^2} \right)^x & t > r. \end{cases} \quad (14)$$

This can be interpreted, that for $t < r$ the magnetization keeps its initial value until the quasiparticles from the defect arrive at $t = r$ and afterwards for $r \ll t \ll L/2$ the decay is given by $m_r^{(+)}(t) \sim t^{-2x}$. This decay involves twice of the magnetization exponent and this behaviour is similar to that of the equilibrium autocorrelation function at the critical point.

In order to check the conformal result in Eq.(14) we have calculated the time-dependence of the magnetization in finite chains of length up to $L = 256$. For the largest chain and for different values of r the relaxation of the magnetization is shown in Fig.2. In agreement with the quasi-particle picture and with the results of conformal invariance the local magnetization stays unchanged until $t < r$, which is followed by a fast decrease. Due to the finite size of the system the magnetization has a finite, L -dependent limiting value and for $t > L/2$ the magnetization starts to increase.

We have studied in more detail the behavior of the magnetization at the defect: $l = L/2$, i.e. for $r = 1$. For short times, $1 \gg t \gg L/2$, the decay is compatible

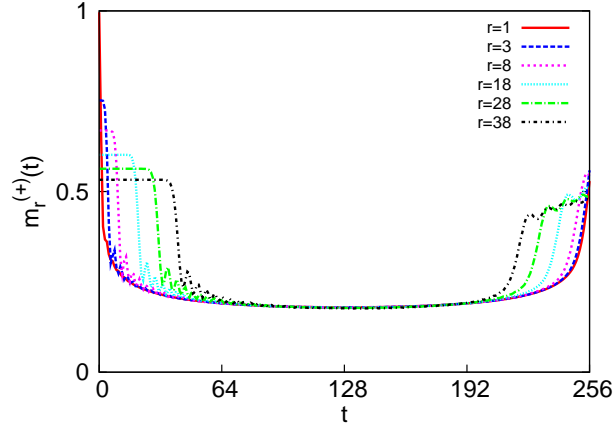


Figure 2. (Color online) Temporal evolution of the magnetization at the critical point after a local quench having fixed spins at the defect in a finite system of length $L = 256$.

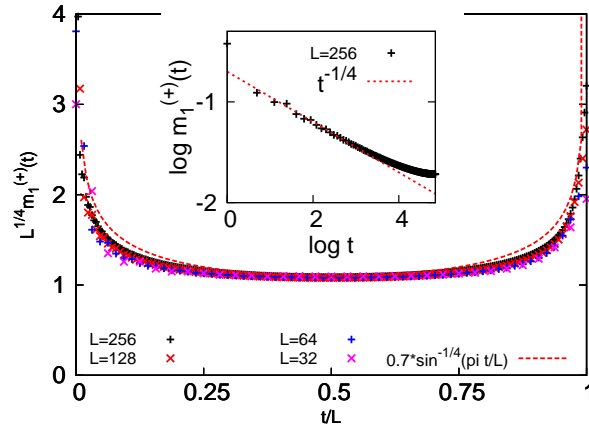


Figure 3. (Color online) Temporal evolution of the magnetization at the defect after a local quench from a fixed spin at the critical point. In the main panel the scaled profiles are shown for different values of L , where the curve with the dashed line is given in Eq.(15). In the inset the log-log plot of $m_1^{(+)}(t, L)$ is shown for $L = 256$, where the conformal prediction for $L \rightarrow \infty$ is given by the dashed straight line.

with the conformal prediction: $m_1^{(+)}(t) \sim t^{-1/4}$ is seen in the inset of Fig.3 in which the magnetization is shown as a function of time in a log-log plot. For longer time the boundaries of the chain start to influence the relaxation and the critical defect magnetization is expected to satisfy the scaling behavior: $m_1^{(+)}(t, L) = b^{-2x} m_1^{(+)}(t/b^z, L/b)$, when lengths are rescaled by a factor $b > 1$. In this relation the dynamical exponent is $z = 1$ and by taking the scaling factor as $b = t$ in the limit $L \gg t$ we recover the conformal result: $m_1^{(+)}(t) \sim t^{-2x}$. It is more interesting to take $b = L$, when one obtains: $m_1^{(+)}(t, L) = L^{-2x} \mu_1^{(+)}(t/L)$. Here the scaling function $\mu_1^{(+)}(\tau)$ for small $\tau = t/L$ behaves as: $\mu_0^{(+)}(\tau) \sim \tau^{-2x}$. Numerical results for the scaling function for different values of L are shown in the main panel of Fig.3, which is found to be well

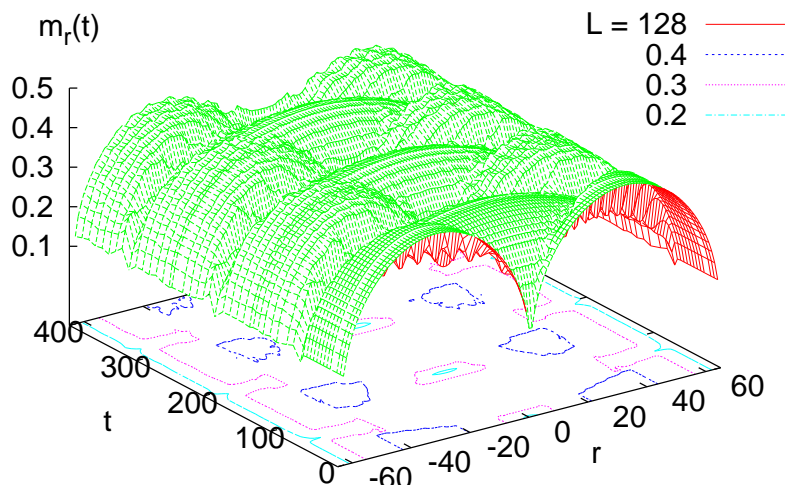


Figure 4. (Color online) Temporal evolution of the local magnetization profiles at the critical point after a local quench with free boundary conditions in the initial state.

approximated by the function $B [\sin(\pi\tau)]^{-2x}$, thus we have the conjecture:

$$m_1^{(+)}(t, L) \propto L^{-2x} \left[\sin \left(\pi \frac{t}{L} \right) \right]^{-2x}. \quad (15)$$

3.2.2. Free-spin boundary condition In this section in the initial state the two half chains have free boundary conditions, which means that in Eq.(9) we have $h_{L/2} = h_{L/2+1} = 1$ and $J_{L/2} = 0$. In this settings no conformal results are available, therefore we study numerically the properties of the profiles of the off-diagonal order parameter, $m_r(t)$ in Eq.(11) in finite systems. The results are shown for $L = 128$ in Fig. 4.

Initially (at $t = 0$) the ground state magnetization profiles are identical and independent in both disconnected parts of the system. The functional form is known from conformal invariance [40] and the complete profile has the finite size scaling form

$$m_r(t = 0, L) \propto L^{-x} \left| \sin \frac{2\pi r}{L} \right|^{x_s - x}. \quad (16)$$

Close to the defect, i.e. for $|r| \ll L/2$ the behavior of the profile follows from the scaling relation, that $m_r(t = 0, L) = b^{-x} m_{r/b}(t = 0, L/b)$, with a rescaling factor, $b > 1$. Now taking $b = L$, we arrive to the form: $m_r(t = 0, L) = L^{-x} \tilde{m}(r/L)$, where the scaling function, $\tilde{m}(\rho)$ for small argument behaves as $\tilde{m}(\rho) \sim \rho^{x_s - x}$. This is compatible with the conformal result in Eq.(16), if we replace ρ by its sinusoidal extension: $\sin(2\pi\rho)$.

In Fig. 4 one observes a quasi-periodic time-dependence of the profile with the characteristic initial double peak being exchanged against a single peak at times $T = L/2, 3L/2, \dots$ and re-occurring at times $T = L, 2L, \dots$. Let us focus first on the time-dependence of the magnetization at the central cite, $m_1(t, L)$, which is expected to

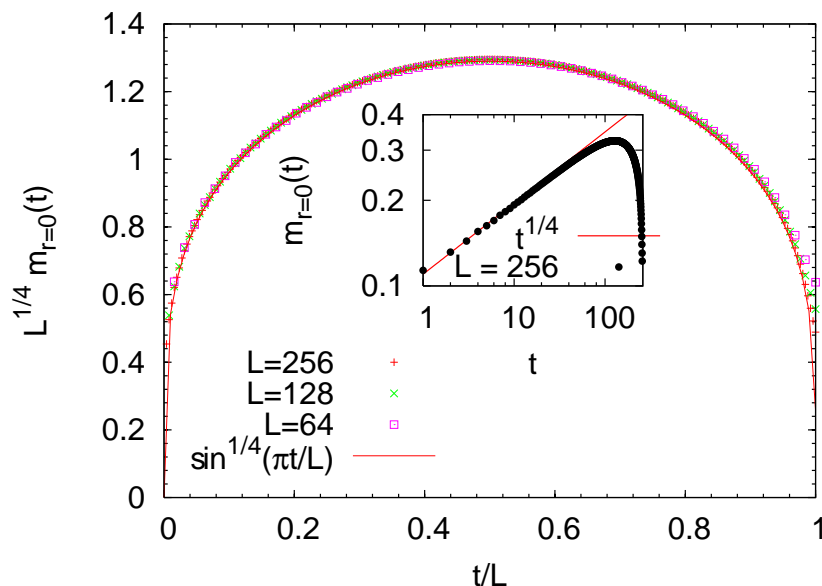


Figure 5. (Color online) Scaling plot of the local magnetization at the defect, $m_0(t)$, after a local quench at criticality for different system size L . The conjectured result in Eq.(17) is shown by a full line. **Inset:** Log-log plot of $m_0(t)$ vs. t for $L = 256$. The straight line is proportional to $t^{1/4}$.

satisfy the same type of scaling relation as $m_1^{(+)}(t, L)$, thus: $m_1(t, L) = b^{-2x} m_1(t/b, L/b)$. As before taking $b = L$ we arrive to: $m_1(t, L) = L^{-2x} \tilde{\mu}_1(t/L)$, where the scaling function, $\tilde{\mu}_1(\tau)$, for small argument should behave as $\tilde{\mu}_1(\tau) \sim \tau^{x_s-2x}$. In this way we obtain: $m_1(t, L) = L^{-x_s} t^{x_s-2x}$, which is in agreement with the L -dependence of the magnetization at the defect at $t = 0$, see in Eq.(16). Furthermore we have for the relaxation for small times: $m_1(t) \sim t^{1/4}$, which agrees well with the numerical data shown in the inset of Fig. 5. The form of the scaling function can be conjectured using the same substitution, $\rho \rightarrow \sin(2\pi\rho)$, as for $t = 0$. In this way we obtain:

$$m_1(t, L) \propto L^{-2x} \left| \sin \frac{2\pi t}{L} \right|^{x_s-2x} \quad (17)$$

Fig. (5) displays a corresponding finite size scaling plot for the first period which shows a good data collapse (a corresponding scaling plot for larger values of t/L is equally good, data not shown) and thus confirms our conjecture (17), which probably can be derived rigorously from conformal invariance.

Next we consider $t = L/2$, when the profile has its maximum at $r = 0$ and it is minimal at the two ends of the chain, $r = \pm L/2$, i.e. at $l = 1$ and $l = L$. Let us consider the profile for small l and use the scaling transformation: $m_l(t/L = 1/2, L) = b^{-2x} m_{l/b}(t/L = 1/2, L/b)$, which leads to the result: $m_l(t/L = 1/2, L) = L^{-2x} \mu(l/L)$, with $b = L$. The scaling function, $\mu(y)$, for small argument is expected to behave in the same way as for $t = 0$, thus $\mu(y) \sim y^{x_s-x}$. Furthermore having the substitution:

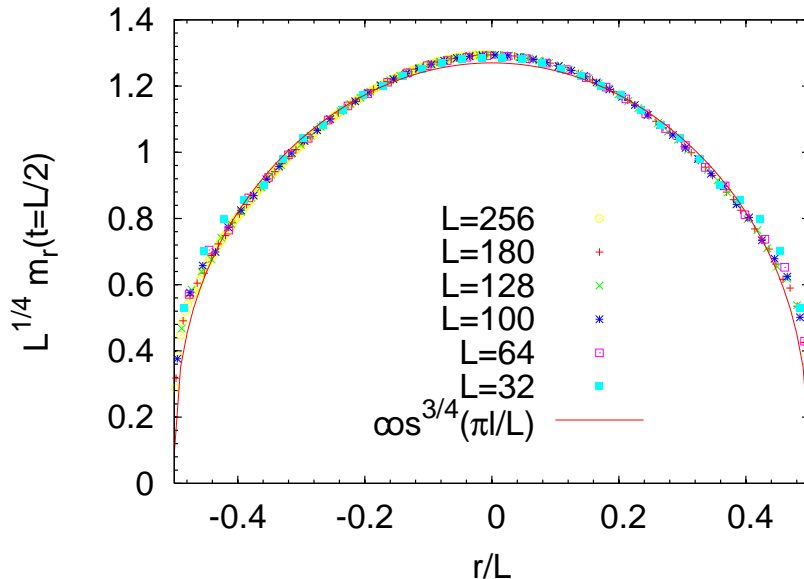


Figure 6. (Color online) Scaling plot of the local magnetization $m_r(t)$ after a local quench at criticality for different system size L at time $t = L/2$, see Eq.(18).

$y \rightarrow \sin(2\pi y)$ we arrive to the conjecture:

$$m_r(t = L/2, L) \propto L^{-2x} \left| \cos \frac{\pi r}{L} \right|^{x_s - x}, \quad (18)$$

where we use the variable r . Fig. 6 displays a corresponding finite size scaling plot which shows a good data collapse and thus supports our conjecture (18).

Combining the scaling forms (17) and (18) the ratio $R = m_{l=L/2}^{(L)}(t = \tau) / m_{l=\tau}^{(L)}(t = L/2)$ is given by

$$R = \left(\sin \pi \frac{\tau}{L} \right)^{-x}. \quad (19)$$

3.3. Spatial correlations

The spatial correlation function, $C_t(r_1, r_2)$ in Eq.(5), has also been studied by conformal field theory [27] and various analytical predictions have been made in an *infinite* system in the continuum limit. In this section we will compare our results for *finite* lattice systems with free boundaries with these predictions. We note that before the quench the two halves of the system are disconnected and free, i.e. $h_{L/2} = h_{L/2+1} = 1$ and $J_{L/2} = 0$. Without the restriction of generality we take $r_1 > |r_2| > 0$ and consider two cases: 1) both sites of reference are at the same side of the defect ($r_2 > 0$), and 2) the two sites are at different side of the defect ($r_2 < 0$).

Case 1: $r_2 > 0$ For short times, $t < r_2 (< r_1)$, the behavior of the correlation function can be obtained in the quasi-particle picture. In this case the quasi-particles (which can be called as signals) starting at the defect and propagating with a speed $v = 1$ does not reach any point of reference, thus the correlations keep their initial

value: $C_t(r_1, r_2) = C_0(r_1, r_2) \propto |r_1 - r_2|^{-2x}$. This result follows also from conformal field theory and consistent with our numerical data depicted in Fig. 7 a and b.

For intermediate times, $r_2 < t < r_1$, the signals reach the closest site at r_2 but not yet the remote site at r_1 , see 7 a and b. The prediction from conformal field theory [27] is

$$C_t(r_1, r_2) = \left\{ \frac{(r_1 + r_2)(r_2 + t)\epsilon}{(r_1 - r_2)(r_1 - t)4r_1(t^2 - r_2^2)} \right\}^x \times F\left(\frac{2r_1(r_2 + t)}{(r_1 + r_2)(r_1 + t)}\right) \quad (20)$$

with

$$F(\eta) = \left(\sqrt{1 + \sqrt{\eta}} - \sqrt{1 - \sqrt{\eta}} \right) / \sqrt{2} \sim \sqrt{\eta} \quad \text{for } \eta \rightarrow 0 \quad (21)$$

and ϵ is the regularization parameter in Eq.(12). In Fig. 7b a comparison with our numerical data for a specific r_1 and r_2 is shown. As expected for a lattice model our data display characteristic oscillations in the considered regime around the monotonous continuum result (20).

For a more quantitative comparison we first look at the asymptotic behavior of $C_t(r_1, r_2)$ for fixed small t and r_2 . The conformal field theory predicts according to (20) and (21)

$$C_t(r_1, r_2) \propto r_1^{-2x-x_s} = r_1^{-3/4} \quad \text{for } t < r_2 \ll r_1 \quad (22)$$

which agrees well with our lattice result as shown in Fig. 7c. Moreover, for fixing the ratios $\rho_2 = r_2/t < 1$ and $\rho_1 = r_1/t > 1$ (20-21) predicts in the limit $t \rightarrow \infty$

$$C_t(r_1, r_2) \propto t^{-3x} = t^{-3/8} \quad \text{for } \rho_2 < 1 \rho_1 > 1 t \rightarrow \infty. \quad (23)$$

This is also consistent with our finite lattice data as seen in Fig. 7d for $\rho_2 = 1/2$ and $\rho_1 = 2$.

In the long-time regime, for $t > r_1$ the signals have also reached the remote site at r_1 , and both points of reference has the information of the joining of the two halves of the system. Consequently $C_t(r_1, r_2)$ approaches a time-independent value (c.f. Fig. 20a and b), given by the equilibrium bulk correlation function, which is proportional to $|r_1 - r_2|^{-2x}$.

Case 2: $r_2 < 0$, i.e. the two reference sites are at the different sides of the defect. Initially, at $t = 0$, the two magnetization operators are located in separate, independent subsystems, thus their correlations should vanish. As long as after the quench no signal reaches the site at r_2 (i.e. for $t < |r_2|$) the correlation function should be expected to be zero. (Strictly speaking $C_t(r_1, r_2)$ can be exponentially small, the only contributions coming from signals propagating outside the ‘‘light-cone’’.) This is clearly visible in our results shown in Fig. 8a. Surprisingly this disagrees with the conformal field theory result [27] which predicts

$$C_t(r_1, r_2) = \frac{1}{|4r_1r_2|^x} \cdot F\left(\frac{\epsilon^2 r_1 |r_2|}{(r_1^2 - t^2)(r_2^2 - t^2)}\right) \quad \text{for } t < |r_2|. \quad (24)$$

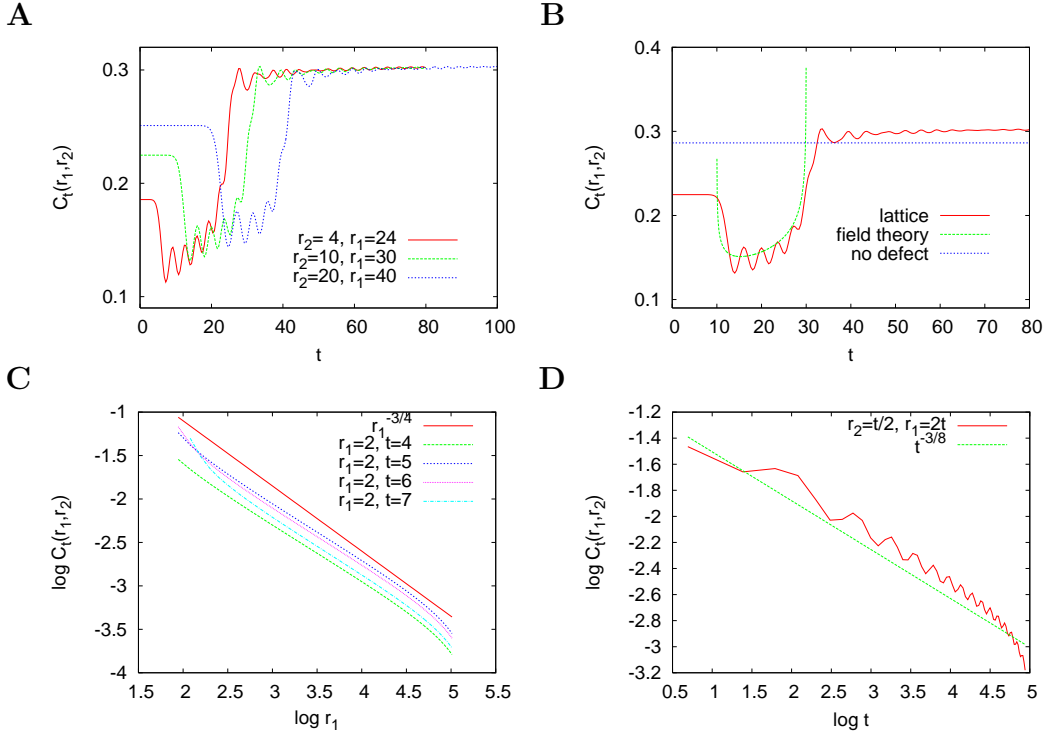


Figure 7. (Color online) **A:** Spatial correlation function $C_t(r_1, r_2)$ as a function of time t for both sites of reference being at the same side of the defect (i.e. $r_1 \geq r_2 > 0$). The system size is $L = 256$, as in the other panels. **B:** Comparison of the data of A for $r_2 = 10$, $r_1 = 30$ with the conformal field theory result (20). **C:** $C_t(r_1, r_2)$ in the intermediate time regime ($r_2 < t < r_1$) for small r_2 and t as a function of r_1 . In the limit $r_1 \rightarrow \infty$ this should approach $r_1^{-3/4}$ according to the conformal field theory result (22). **D:** $C(r_1, r_2; t)$ in the intermediate time regime for $r_2 = t/2$ and $r_1 = 2t$ as a function of t that should decay as $t^{-3/8}$ according to the conformal field theory result (23).

This could be rectified by setting $\epsilon = 0$, but this would be at variance with the results for $r_2 > 0$, for which the regularization parameter should be non-vanishing. The problem with the conformal derivation could be related to the fact, that in the transformation (12) points in the z plane with $\text{Re}(z_2) = r_2 < 0$ and $|r_2| \gg \epsilon$ are transformed to $|w_2| \ll \epsilon$. However, the scaling form of the correlation function in the semi-infinite w -plane is valid only in the continuum limit, i.e. for $\text{Re}(w_2) \gg 1$.

After the signals reach the site at r_2 , i.e. for $|r_2| < t < r_1$, the conformal field theory prediction is [27]

$$C_t(r_1, r_2) = \left(\frac{(r_1 + r_2)(r_2 + t)\epsilon}{(r_1 - r_2)(r_1 - t)4r_1(t^2 - r_2^2)} \right)^x \times F \left(\frac{2r_1(r_2 + t)}{(r_1 + r_2)(r_1 + t)} \right) \quad \text{for } |r_2| < t < r_1. \quad (25)$$

In Fig. 8b a comparison with our numerical data for a specific r_1 and r_2 is shown. As expected for a lattice model our data display characteristic oscillations in the considered regime around the monotonous continuum result (25).

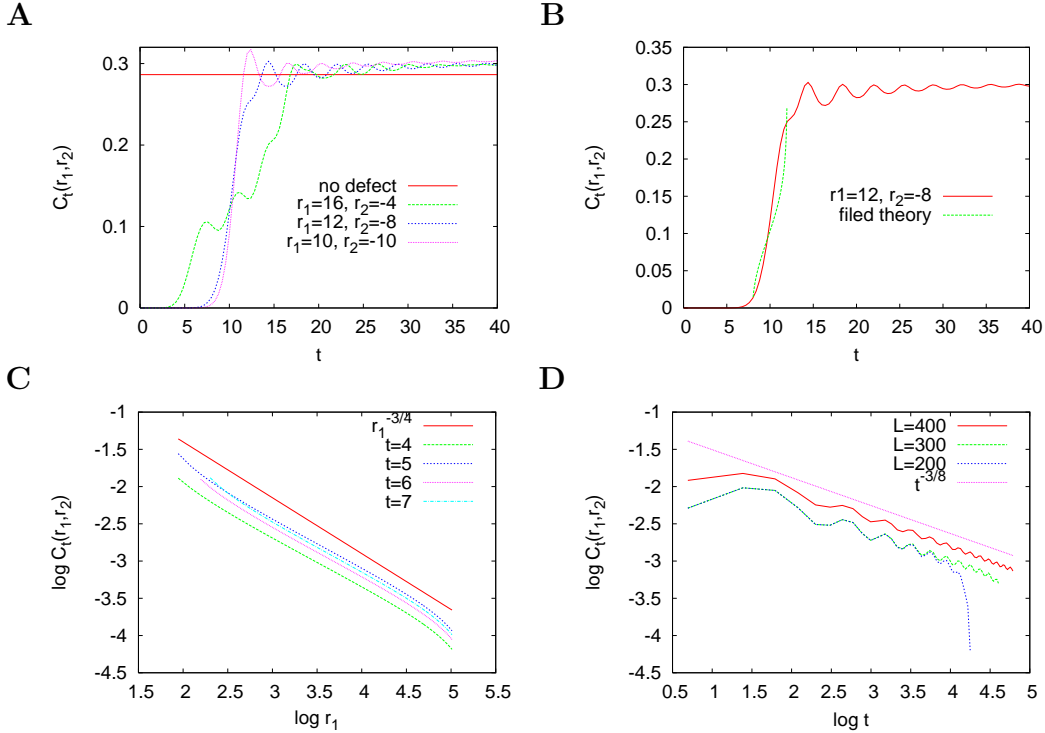


Figure 8. (Color online) **A:** Spatial correlation function $C_t(r_1, r_2)$ as a function of time t for the two sites of reference being at different sides of the defect: $r_1 > 0, r_2 < 0$ ($r_1 \geq |r_2|$). The system size is $L = 256$, as in the other panels. **B:** Comparison of $C_t(r_1, r_2)$ with the conformal field theory result (25). **C:** $C_t(r_1, r_2)$ for small $|r_2|$ and t as a function of r_1 . In the limit $r_1 \rightarrow \infty$ this should approach $r_1^{-3/4}$ according to the conformal field theory result (22). **D:** $C_t(r_1, r_2)$ for $r_2 = t/2$ and $r_1 = 2t$ as a function of t that should decay as $t^{-3/8}$ according to the conformal field theory result (23).

For fixed small t and r_2 the conformal field theory predicts according to (25) and (21) again for $C_t(r_1, r_2)$ the asymptotic r_1 -behavior (22) as in the case $r_2 > 0$. This agrees well with our lattice result as shown in Fig. 8c. Moreover, for fixed $\rho_2 = r_2/t > -1$ and $\rho_1 = r_1/t > 1$ (25) predicts in the limit $t \rightarrow \infty$ the same asymptotic t -behavior (23) as in the case $r_2 > 0$. This is also in agreement with our lattice result as shown in Fig. 8d. Finally for $t > r_1$ the signal has also reached the site at r_1 and $C_t(r_1, r_2)$ approaches again the time-independent equilibrium bulk value (c.f. Fig. 8), which is proportional to $|r_1 - r_2|^{-2x}$.

Summarizing our results confirm the predictions of the conformal field theory [27] for the spatial correlation after a local quench at the critical point, except for the case $r_2 < 0, t < |r_2|$.

3.4. Autocorrelations

We have also calculated the autocorrelation function, $G_r(t, 0)$, as defined in Eq.(4). In the following for simplicity we shall omit the second argument and use the notation $G_r(t)$. Using the quasi-particle picture we have the following expectations. Before the

signal reaches the reference point, $t < r$, the autocorrelation function is the same as in the equilibrium bulk system, thus asymptotically $G_r(t) \propto t^{-2x/z} = t^{-1/4}$. For $t > r$, when the signal has passed the reference point the equilibrium bulk decay of $G_r(t)$ should continue, thus in the complete time-window this behavior is observable.

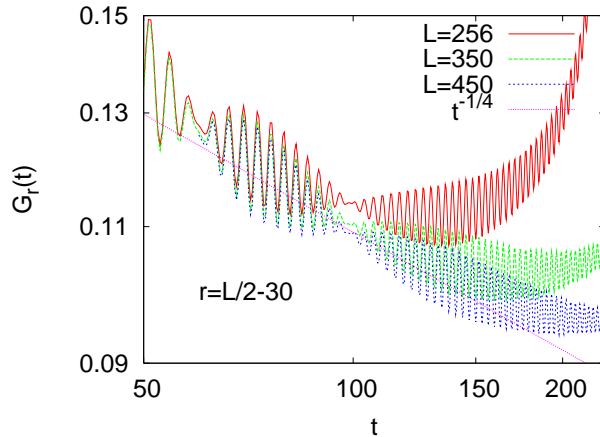


Figure 9. (Color online) Autocorrelation function $G_r(t)$ after a critical quench for different system sizes. The straight line corresponds to the equilibrium power law $t^{-1/4}$.

Our lattice results in Fig. 9 are in agreement with these expectations. In a finite lattice of length L the autocorrelation function has a minimal value of $\sim L^{-1/4}$.

4. Quench in the ferromagnetic phase

In equilibrium in the ferromagnetic (FM) phase ($h < 1$) there is spontaneous order and the bulk m_b and the surface, m_s , magnetizations are given by:

$$m_b = (1 - h^2)^{x\nu}, \quad m_s = (1 - h^2)^{x_s\nu}, \quad (26)$$

respectively (the correlation length exponent is $\nu = 1$). The magnetization profile has an exponential variation in the surface region, the size of which is given by: $\xi_s \sim (1 - h)^{-1}$, close to the critical point. Here we follow the same protocol as in Sec.3.2.2: for $t < 0$ we cut the system into two halves with free boundary conditions, which are then (at $t = 0$) joined together with the coupling $J_{L/2} = J = 1$. We measure the temporal evolution of the magnetization profile, $m_r(t)$, as defined in Eq.(11). The finite lattice results are depicted in Fig. 10 for $h = 0.5$ and $L = 128$. In the initial state the magnetization profile ($m_r(t = 0)$) is essentially constant and given by m_b , except close to the boundaries and to the center. For $t > 0$ one observes again a quasi-periodic pattern and the period of time $T(h)$ is found to increase with increasing L and decreasing field h . It turns out that the spatio-temporal evolution of the profile can be understood even quantitatively within a quasi-classical picture.

As elaborated in [41] within the FM phase the dynamics of the local order parameter in a system with boundaries after a *global* quench is very well described by a quasi-

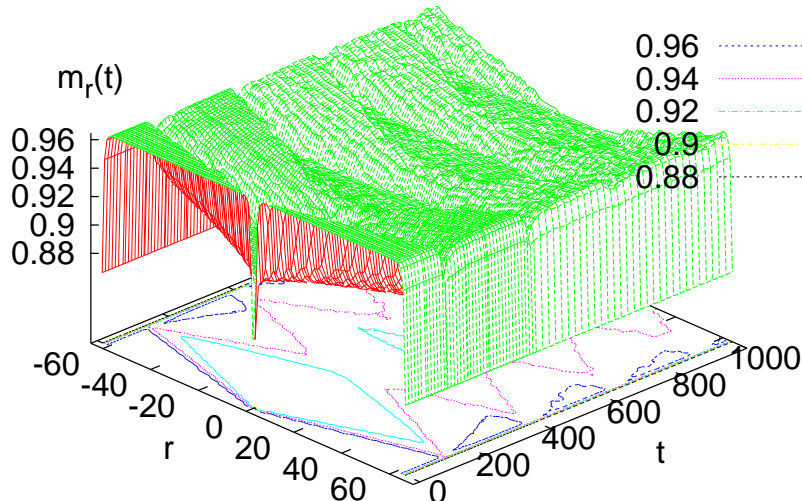


Figure 10. (Color online) Temporal evolution of the local magnetization profiles after a local quench within the ordered (FM) phase, here $h = 0.5$, $L = 128$.

particle (QP) picture, where QPs are kinks that move with velocity $\pm v_p$ through the system. The QP energy is

$$\epsilon_p = \sqrt{1 + h^2 - 2h \cos(p)} \quad (27)$$

with $p = (2n - 1)\pi/2L$ ($n = 1, \dots, L$) and the QP velocity is

$$v_p = \frac{\partial \epsilon_p}{\partial p} = \frac{h \sin(p)}{\epsilon_p}. \quad (28)$$

The maximum velocity is given by:

$$v_{\max}^2 = \left[\sqrt{(1 + h^2)^2 + 12h^2} - (1 + h^2) \right] / 6, \quad (29)$$

for small h it is $v_{\max} \approx h$.

Consider now a QP, or kink, with momentum p . It moves uniformly with velocity v_p until it reaches one of the boundaries, where it is reflected and moves with velocity $-v_p$ thereafter, and so forth. The trajectory of the kink is periodic in time, after a time $2T_p$ with

$$T_p = L/v_p \quad (30)$$

(including a reflection at the right and left boundary) it returns to the starting point x_0 with the initial direction and velocity v_p . After a *global* quench QPs emerge pairwise at random positions x_0 with velocities $+v_p$ and $-v_p$ [18, 41] and therefore we assume that after the *local* quench studied here QPs emerge also pairwise, but exclusively at the central site, where the defect is located before the quench.

The time dependent decay of the local magnetization $m_r(t)$ at a position r is then determined by the probability q with which any given kink trajectory passes until time t the site r an odd (!) number of times: Each passage of one of the two trajectories flips the spin at site r and an even number of flips does not change the magnetization of site r . Once $q(t)$ is known the magnetization is given by

$$m_r(t) = m_r(t=0) \cdot \exp(-2q(t)). \quad (31)$$

The probability $q(t)$ is expressed as

$$q(t) = \frac{1}{\pi} \int_0^\pi dp f_p(h) q_p(t) \quad (32)$$

where $q_p(t)$ is the probability that any given QP trajectory passes the site r an odd number of times, and $f_p(h)$ is the probability with which QPs with momentum p are generated (per site), and we take assume that it is identical to f_p after a global quench. This is given for small h as [41]:

$$f_p(h) = \frac{1}{4} h^2 \sin^2(p) \quad (33)$$

To calculate q_p one concentrates first on times $t < 2T_p$ and on lattice site $r < 0$ - the whole profile is of course symmetric with respect to a reflection at the center $m_r(t) = m_{-r}(t)$. The QPs emerging at the central site $r = 1$ and moving to the left ($v_p < 0$) pass the site r two times (once before the reflection at the left boundary and once after the reflection) before they return (now with $v_p > 0$) to their starting point. These two times are $t_1 = |r|/v_p$ and $t_2 = T_p - t_1$. Therefore the probability that this QP trajectory passes r at times $t < T_p$ exactly once is

$$q_p^- = \begin{cases} 0 & t < t_1 \\ 1 & t_1 < t < t_2 \\ 0 & t_2 < t < T_p \end{cases} \quad (34)$$

The associated partner (of the QP pair) that moves to the right ($v_p > 0$) passes the site r only after reflection at the right boundary and returns to the starting point, at times $t_3 = T_p + t_1$ and $t_4 = 2T_p - t_1$. Therefore the probability that this QP trajectory passes r at times $t < 2T_p$ exactly once is

$$q_p^+ = \begin{cases} 0 & t < t_3 \\ 1 & t_3 < t < t_4 \\ 0 & t_4 < t < 2T_p \end{cases} \quad (35)$$

For $t > 2T_p$ one makes use of the T_p -periodicity of $q_p(t)$:

$$q_p(t + 2nT_p) = q_p(t), \quad (n = 1, 2, \dots). \quad (36)$$

With (32), (33), (34-36) one obtains $m_l(t)$ via numerical integration (or summation over the discrete p -values for a lattice of finite size L), where we take the exact profile before the quench ($m_l(t=0)$).

In Fig. 11 the comparison of this QP calculation with our exact data is shown. Fig. 11A displays the dynamical evolution of the local magnetization at $h = 0.2$ close to the

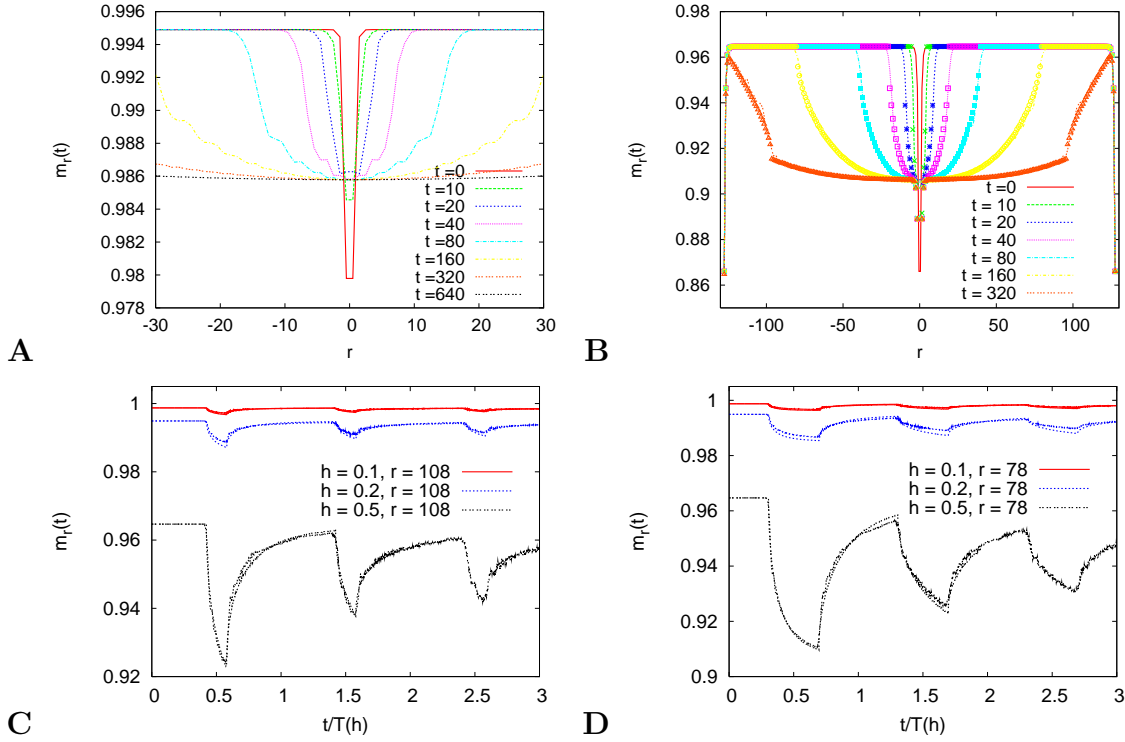


Figure 11. (Color online) Local order parameter $m_l(t)$ within the FM phase ($h < 1$) and comparison with QP calculation. **A:** $m_r(t)$ at $h = 0.2$ as a function of the distance r from the defect for different fixed times t . **B:** $m_l(t)$ at $h = 0.5$ as a function of l for different fixed times ($L = 256$, the defect is at $l = 128$). The full lines are the exact data and the points are the predictions of the QP calculation. **C-D:** $m_l(t)$ for different fields $h < 1$ as a function of the rescaled time $t/T(h)$, where $T(h) = L/v_{\max}(h) = L/h$, i.e. $T(h = 0.5) = 512$, $T(h = 0.2) = 2560$, and $T(h = 0.1) = 5120$. The exact data and the QP prediction can be discriminated by the smoother behavior of the latter.

defect. The system size, $L = 256$, is sufficiently large such that the boundary effects are not yet visible for the times shown and the data are representative for an infinite system. One sees that the initial magnetization drop at the defect (the defect spins are surface spins at $t = 0$) is quickly filled and the profile approaches a constant magnetization $\widetilde{m}_b = \lim_{L, t \rightarrow \infty} m_r(t)$. Since the probability $q_p(t)$ for a QP with momentum p to pass any site in the bulk is 1 in the limit $L \rightarrow \infty$ and $t \rightarrow \infty$ the bulk magnetization is predicted by the QP picture, according to (32) and (31), to be

$$\widetilde{m}_b = m_b \exp(-1/\xi), \quad (37)$$

with

$$\frac{1}{\xi} = \frac{1}{\pi} \int_0^\pi dp f_p(h). \quad (38)$$

ξ is identical with the nonequilibrium correlation length measured during *global quench*, as defined in Eq.(6). For $f_p(h)$ as in Eq.(33), which is exact for small h it is given by: $1/\xi = h^2/4$. For larger values of h corrections to the kink-like excitations should be summed, which leads to the value [42, 20]: $1/\xi = -\ln \left[(1 + \sqrt{1 - h^2})/2 \right]$. For $h = 0.2$

one gets $\widetilde{m}_b = 0.985$ which agrees well with the approximately constant magnetization at $t = 640$ in Fig. 11A. We checked that also for larger values of h the QP prediction for the asymptotic bulk magnetization \widetilde{m}_b in eq.(37) is good.

Fig. 11B compares the exact data for the local magnetization profile of a finite system for different times after the quench with those of the QP prediction at $h = 0.5$. The agreement is very good for the times shown and a few sites away from the defect ($r = |L/2 - l| > 5$). The rapid filling of the initial sharp dip of the profile at the center (see Fig. 11A) is not correctly captured by the present QP picture. To understand this process one should assume, that the QP-s are emitted in a region of size ξ_s around the defect and these QP-s are quantum entangled and these correlated particles are responsible for the rapid increase of the magnetization at the defect.

The predicted (quasi)-period is governed by the maximum QP velocity and given by

$$T(h) = L/v_{\max} \approx L/h . \quad (39)$$

This agrees well with the dynamical behavior of $m_l(t)$ shown in 11 C-D displaying the exact data and the QP prediction for $m_l(t)$ at fixed sites l for different fields $h < 1$ as a function of the rescaled time $t/T(h)$. The agreement for the sites shown is good, at longer times close to the defect ($l \approx L$) deviations occur (see Fig. 11D) due to the mechanism described above.

5. Quench in the paramagnetic phase

In the paramagnetic phase ($h > 1$) the magnetization is vanishing in the thermodynamic limit, however, in a finite system there is a finite, L -dependent magnetization. Its temporal evolution for $h = 2$ is depicted in Fig. 12 for $L = 128$. In contrast to the dynamics at the critical point (c.f. Fig. 4) the evolution of $m_l(t)$ is not periodic in the paramagnetic phase and approaches a stationary profile characteristic for the system without defect.

Our results for the spatial correlation function $C_t(r_1, r_2)$ within the paramagnetic phase are depicted in Fig. 13. We find that for fixed r_1 and r_2 an asymptotic power law in t with an exponent close to $3/2$:

$$C_t(r_1, r_2) \propto t^{-3/2} \quad \text{for } t \gg r_1, |r_2| . \quad (40)$$

Finally the autocorrelation function after a local quench in the paramagnetic phase decays as in the ground state without a defect, i.e.

$$G_t(r) \propto t^{-1/2} . \quad (41)$$

see Fig. 14.

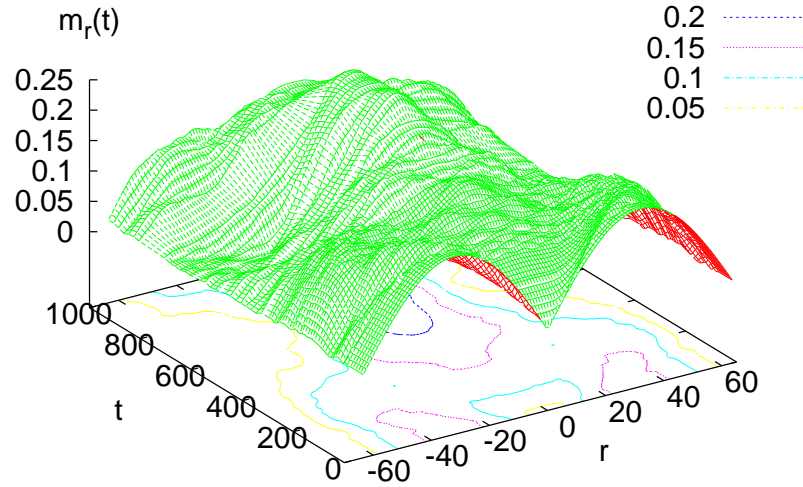


Figure 12. (Color online) Temporal evolution of the local magnetization profiles after a local quench within the disordered (PM) phase, here $h = 2$, $L = 128$.

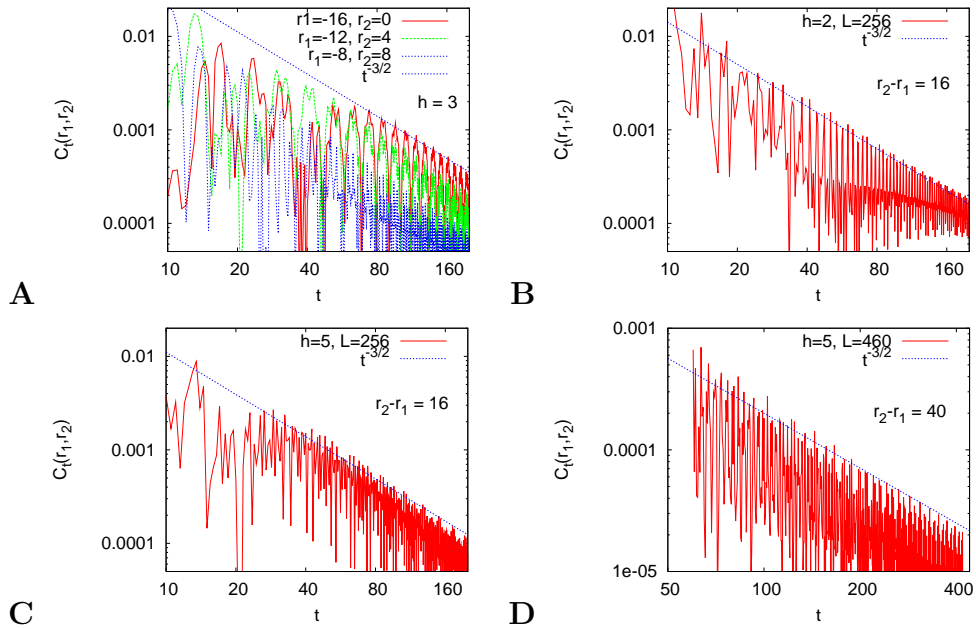


Figure 13. (Color online) Spatial correlation function $C_t(r_1, r_2)$ as a function of t for local quenches in the paramagnetic phase ($h > 1$) in a log-log plot. The straight lines correspond to the power law $t^{-3/2}$. **A:** Different pairs of (r_1, r_2) with the same spatial difference at $h = 3$ (L is 256). **B:** $h = 2$, $L = 256$. **C:** $h = 5$, $L = 256$. **D:** $h = 5$, $L = 460$.

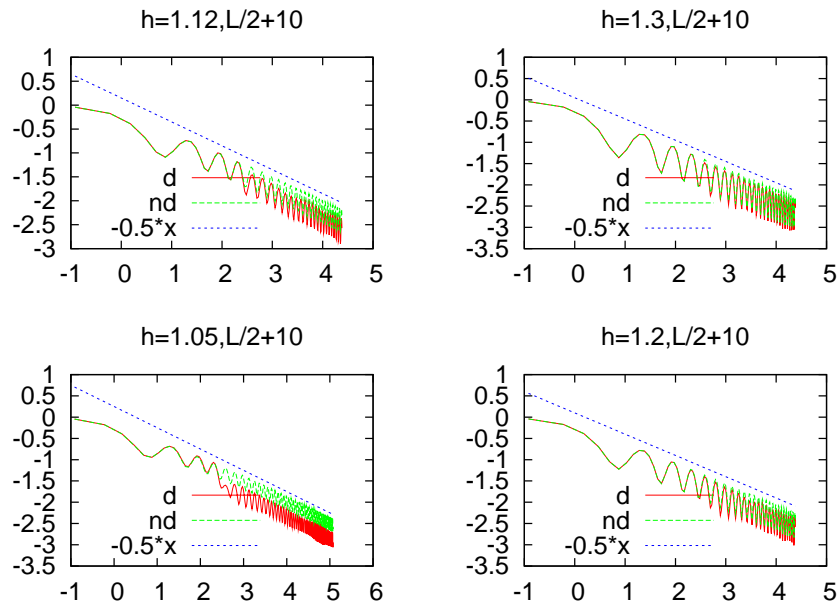


Figure 14. (Color online) Autocorrelation function $G_r(t)$ after a quench in the paramagnetic phase for $r = 10$ (i.e. for a site in a distance 10 from the defect) for different values of h in comparison with $G_r(t)$ for a system without defect (“nd”).

6. Conclusions

We have studied the temporal evolution of different observables in the transverse Ising chain following a local quench: for $t < 0$ the system consisted of two disconnected halves which are joined together for $t > 0$ with the uniform bulk coupling, $J_{L/2} = 1$. We have measured the magnetization profile, $m_r(t)$, as well as the correlation, $C_t(r_1, r_2)$ and the autocorrelation function, $G_r(t_1, t_2)$. We have concentrated on the properties of local quench in the critical state, but some calculations are also performed in the ferromagnetic and in the paramagnetic phases, too.

For critical local quench several conjectures about $m_r(t)$ and $C_t(r_1, r_2)$ are known through conformal field theory, which are valid in the thermodynamic limit and in the continuum approximation. Our exact finite lattice results have confirmed the conformal conjectures, except for the early time behavior of the correlation function in which the two reference points are at different sides of the defect. We have also studied systematically the finite-size effects, in particular we have made conjectures about the form of the magnetization profiles, both in space Eq.(18) and time Eq.(17), which probably can be derived in some way, e.g. through conformal field theory.

Our results are explained within the frame of a quasi-particle picture, in which during the quench kink-like excitations are created at the defect, which move semi-classically, with a momentum-dependent velocity and result in the reduction of the order-parameter in the system. In the ferromagnetic phase this type of semi-classical calculation has lead to exact results, at least for a small transverse field, h . We expect,

however, that following the same method as in the case of global quench, one can sum the higher order contributions and in this way one obtains exact results about the stationary value of the magnetization profile for general value of $h < 1$. This involves the non-equilibrium correlation length, ξ , as measured at a global quench, see Eq.(37).

Our investigations can be extended and generalized in different directions. First, one can consider another quantum spin chains, for which the conformal conjectures at the critical point are expected to be satisfied in the same way as for the transverse Ising chain. In the ferromagnetic phase the relation in Eq.(37) is expected to be valid and in this way one can measure the non-equilibrium correlation length in an independent procedure. A second way to generalize our results is to use different forms of the local quench. One possibility is to use a non-zero defect coupling between the two subsystems in the initial state and/or to have a non-uniform defect coupling, $J_{L/2} \neq J = 1$, in the final state. In the transverse Ising chain the local critical exponents are continuous function of the strength of the defect [43, 44, 45], so that x_s for a decoupled system should be replaced by a defect exponent, x_d . Finally, we can also study local defects with a more complicated structure, which involve several lattice sites.

Acknowledgments:

One of us (U.D.) is grateful to the Alexander von Humboldt Society for a fellowship with which this work was performed at the Saarland University. This work has furthermore been supported by the Hungarian National Research Fund under grant No OTKA K62588, K75324 and K77629 and by a German-Hungarian exchange program (DFG-MTA). We thank P. Calabrese for useful correspondence.

References:

- [1] M. Rigol, A. Muramatsu, and M. Olshanii, Phys. Rev. A **74**, 053616 (2006).
- [2] M. Rigol, V. Dunjko, V. Yurovsky, and M. Olshanii, Phys. Rev. Lett. **98**, 050405 (2007).
- [3] M. A. Cazalilla, Phys. Rev. Lett. **97**, 156403 (2006).
- [4] P. Calabrese and J. Cardy, Phys. Rev. Lett. **96**, 136801 (2006).
- [5] P. Calabrese and J. Cardy, J. Stat. Mech. P06008 (2007).
- [6] S. Sotiriadis and J. Cardy, Phys. Rev. B **81**, 134305 (2010).
- [7] A. Lamacraft, Phys. Rev. Lett. **98**, 160404 (2007).
- [8] A. M Läuchli and C. Kollath, J. Stat. Mech. P05018 (2008).
- [9] T. Barthel and U. Schollwöck, Phys. Rev. Lett. **100**, 100601 (2008).
- [10] M. Cramer, C. M. Dawson, J. Eisert, and T. J. Osborne, Phys. Rev. Lett. **100**, 030602 (2008).
- [11] M. Kollar and M. Eckstein. Phys. Rev. A **78**, 013626 (2008).
- [12] A. Flesch, M. Cramer, I. P. McCulloch, U. Schollwöck, and J. Eisert. Phys. Rev. A **78**, 033608 (2008).
- [13] M. Cramer, A. Flesch, I. P. McCulloch, U. Schollwöck, and J. Eisert. Phys. Rev. Lett. **101**, 063001 (2008).
- [14] P. Barmettler, M. Punk, V. Gritsev, E. Demler, and E. Altman, Phys. Rev. Lett. **102**, 130603 (2009); New J. Phys. **12**, 055017 (2010)
- [15] G. Roux, Phys. Rev. A **79**, 021608 (2009).
- [16] D. Fioretto and G. Mussardo, New J. Phys. **12**, 055015 (2010).
- [17] V. Gritsev, E. Demler, M. Lukin, and A. Polkovnikov, Phys. Rev. Lett. **99**, 200404 (2007).
- [18] D. Rossini, A. Silva, G. Mussardo, and G. E. Santoro, Phys. Rev. Lett. **102**, 127204 (2009); D. Rossini, S. Suzuki, G. Mussardo, G. E. Santoro and A. Silva Phys. Rev. B **82**, 144302 (2010).
- [19] F. Iglói and H. Rieger, Phys. Rev. Lett. **106**, 035701 (2011).
- [20] P. Calabrese, F. H. L. Essler, M. Fagotti, arXiv:1104.0154
- [21] M. Greiner, O. Mandel, T. W. Hänsch and I. Bloch, Nature **419**, 51 (2002).
- [22] L. E. Sadler *et al.*, Phys. Rev. Lett. **98**, 160404 (2006).
- [23] B. Paredes *et al.* Nature **429**, 277 (2004); T. Kinoshita, T. Wenger and D. S. Weiss, Science **305**, 1125 (2004).
- [24] T. Kinoshita, T. Wenger and D. S. Weiss, Nature **440**, 900 (2006).
- [25] A. Sachdev and A. P. Young, Phys. Rev. Lett. **78**, 2220 (1997).
- [26] V. Eisler and I. Peschel, J. Stat. Mech. P06005 (2007).
- [27] P. Calabrese and J. Cardy, J. Stat. Mech. P10004 (2007).
- [28] V. Eisler, D. Karevski, T. Platini and I. Peschel, J. Stat. Mech. P01023 (2008).
- [29] G.D. Mahan, *Many-Particle Physics* (New-York, Plenum, 1990).
- [30] F. Iglói, Zs. Szatmári, and Y.-Ch. Lin, Phys. Rev. B **80**, 024405 (2009).
- [31] P. Pfeuty, Ann. Phys. **57**, 79 (1970).
- [32] E. Lieb, T. Schultz, and D. Mattis, Ann. Phys. **16**, 407 (1961).
- [33] E. Barouch and B. McCoy, Phys. Rev. A **2**, 1075 (1970); Phys. Rev. A **3**, 786 (1971); Phys. Rev. A **3**, 2137 (1971).
- [34] C. N. Yang, Phys. Rev. **85**, 808 (1952).
- [35] F. Iglói and H. Rieger, Phys. Rev. Lett. **85**, 3233 (2000).
- [36] J. Cardy, Nucl. Phys. B **240**, 514 (1984).
- [37] J. Cardy, Phys. Rev. Lett. **65**, 1443 (1990).
- [38] T. W. Burkhardt and T. Xue, Phys. Rev. Lett. **66**, 895 (1991).
- [39] M. E. Fisher and P.-G. De Gennes, C. R. Seances Acad. Sci., Ser. B **287**, 207 (1978).
- [40] L. Turban and F. Iglói, J. Phys. A **30**, L105 (1997).
- [41] F. Iglói and H. Rieger, to be published.
- [42] K. Sengupta, S. Powell, and S. Sachdev, Phys. Rev. A **69**, 053616 (2004).
- [43] R. Z. Bariev, Zh. Eksp. Teor. Fiz. **77**, 1217 (1979) [Sov. Phys.-JETP **50**, 613 (1979)]

- [44] B. M. McCoy and J. H. H. Perk, Phys. Rev. Lett. **44**, 840 (1980).
- [45] F. Iglói, I. Peschel, and L. Turban, Advances in Physics **42**, 683 (1993).